A Mammalian H^+ Channel Generated Through Alternative Splicing of the NADPH Oxidase Homolog *NOH-1*

Botond Bánfi,[1,5] Andrés Maturana,[2,3] Stefano Jaconi,[1] Serge Arnaudeau,[2] Terese Laforge,[1] Bhanu Sinha,[4] Erzsébet Ligeti,[5] Nicolas Demaurex,[2]* Karl-Heinz Krause[1]

Voltage-gated proton (H^+) channels are found in many human and animal tissues and play an important role in cellular defense against acidic stress. However, a molecular identification of these unique ion conductances has so far not been achieved. A 191–amino acid protein is described that, upon heterologous expression, has properties indistinguishable from those of native H^+ channels. This protein is generated through alternative splicing of messenger RNA derived from the gene *NOH-1* (NADPH oxidase homolog 1, where NADPH is the reduced form of nicotinamide adenine dinucleotide phosphate).

Voltage-gated H^+ channels (*1*) were first described in snail neurons (*2*) and were further characterized in a variety of mammalian cells (*3–5*). They are unique among ion channels with respect to their extremely high selectivity (*5*), marked temperature dependence (*6*), and unitary conductance, which is three orders of magnitude lower than that of most ion channels (*7, 8*). An H^+ channel protein has not yet been identified, but Arg → His mutations were sufficient to turn the voltage sensor of the *Shaker* K^+ channel into a voltage-gated H^+ conductance (*9*). The critical residues (**R/H**VI**R/H**LV**R/H**) (*10*) are not found among known proteins, but are reminiscent of a motif (**H**SAI**H**TIA**H**) within the predicted third transmembrane domain of $gp91^{phox}$, the electron-transporting subunit of the phagocyte NADPH oxidase (*11, 12*).

By analogy with mitochondrial cytochromes, $gp91^{phox}$ had been postulated to conduct protons to preserve electroneutrality (*13*). This prediction was supported by pH measurements in phagocytes and in $gp91^{phox}$ transfectants (*14–16*), and a mutational analysis suggested a role for the histidines of the third transmembrane domain (*17*). However, normal H^+ currents were observed in resting phagocytes from $gp91^{phox}$-deficient patients (*18*), and a distinct type of H^+ current was activated during assembly of the NADPH oxidase (*19*). Thus, $gp91^{phox}$ might conduct protons within an active oxidase complex, but a separate protein, possibly sharing the $gp91^{phox}$ histidine motif, mediates the H^+ currents of resting phagocytes and other tissues.

A search of expressed sequence tag (EST) databases with the $gp91^{phox}$ third transmembrane domain yielded two cDNA clones coding for a short NH_2-terminal $gp91^{phox}$ homolog, which ended with 35 unrelated amino acids. A further search with the COOH-terminus of $gp91^{phox}$ yielded another cDNA sequence, which suggested the presence of a longer homolog. A search of genomic DNA databases with the EST clones yielded a common gene (*20*), localized to the long arm of the human X chromosome (Xq22, Fig. 1), which we termed *NOH-1* (NADPH oxidase homolog 1). Exon 1 (homologous to exon 1 of $gp91^{phox}$) contained a presumable translation initiation site, whereas exon 13 (homologous to exon 13 of $gp91^{phox}$) contained a stop codon. In 3′ position from exon 13, we identified an additional exon (exon 14) corresponding to the unique COOH-terminus of the short NH_2-terminal homolog.

We next used the reverse transcription polymerase chain reaction (RT-PCR) to amplify the expected products of the *NOH-1* gene (*21*). An exon 1–exon 13 primer pair yielded two PCR products (~1.75 and ~1.6 kb) in the colon carcinoma cell line CaCo-2 (Fig. 2A). An exon 1–exon 14 primer pair yielded a ~0.5-kb band in CaCo-2 cells, HL-60 cells, and leukocytes, but not in HEK-293 cells (Fig. 2A), heart, and skeletal muscle

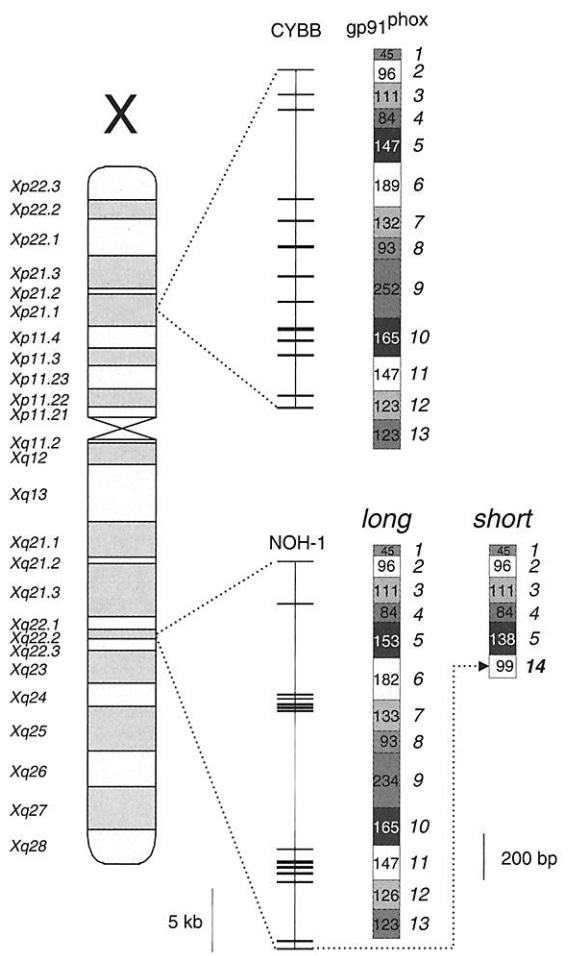

Fig. 1. The *NOH-1* gene generates NOH-1S and NOH-1L through alternative splicing. The *NOH-1* gene, as found in the nonredundant database, localizes to Xq22. The *CYBB* gene (coding for $gp91^{phox}$) localizes to Xp21. Exons are shown as horizontal bars; introns are shown as thin vertical lines. We have identified 14 exons of the *NOH-1* gene; only 13 exons are known for the *CYBB* gene. Exons 1 to 13 constitute NOH-1L; exons 1 to 5 and exon 14 constitute NOH-1S. $gp91^{phox}$ consists of 13 exons, all with lengths similar to the 13 exons of NOH-1L (boxed numbers, coding nucleotides). Arrow indicates the last exon coding the unique NOH-1S COOH-terminus.

[1]Biology of Aging Laboratory, Department of Geriatrics, [2]Department of Physiology, [3]Fondation pour Recherches Médicales, [4]Division of Infectious Diseases, Geneva University Hospitals, Geneva Medical School, CH-1211 Geneva 4, Switzerland. [5]Department of Physiology, Semmelweis Medical University, H-1444 Budapest 8, Hungary.

*To whom correspondence should be addressed. E-mail: Nicolas.Demaurex@medecine.unige.ch

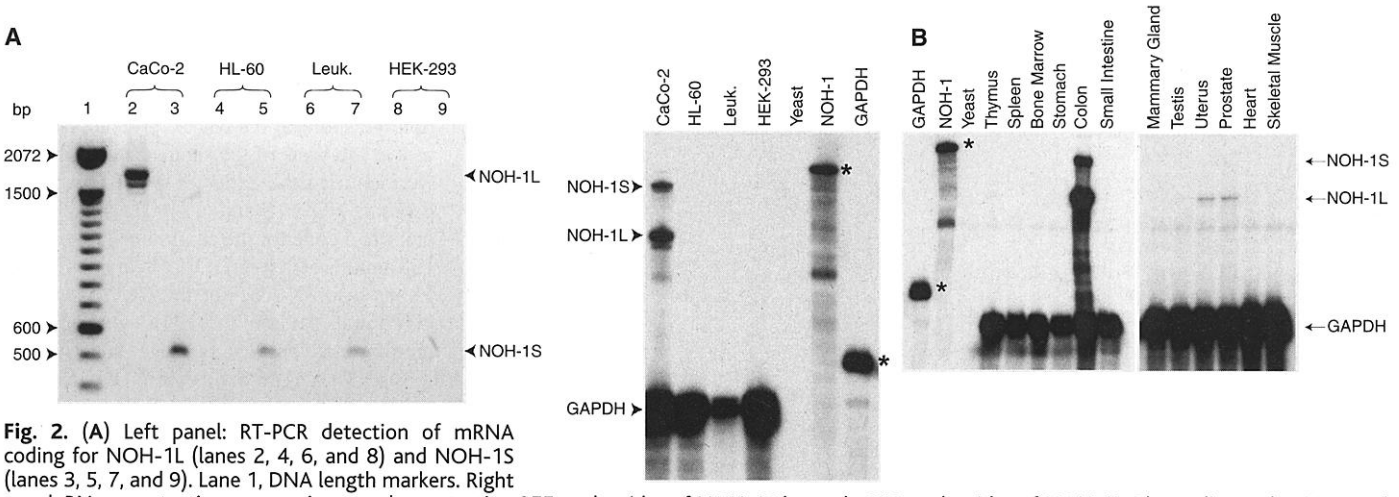

Fig. 2. (**A**) Left panel: RT-PCR detection of mRNA coding for NOH-1L (lanes 2, 4, 6, and 8) and NOH-1S (lanes 3, 5, 7, and 9). Lane 1, DNA length markers. Right panel: RNase protection assay using a probe protecting 355 nucleotides of NOH-1S but only 240 nucleotides of NOH-1L. The undigested *NOH-1* and GAPDH probes are labeled with asterisks (*25*). HL-60 cells were differentiated with DMSO. Human peripheral blood leukocytes (Leuk.) were purified as described (*30*) and included both lymphocytes and granulocytes. (**B**) Tissue distribution of NOH-1L and NOH-1S assessed by RNase protection assay using the probes described in (A).

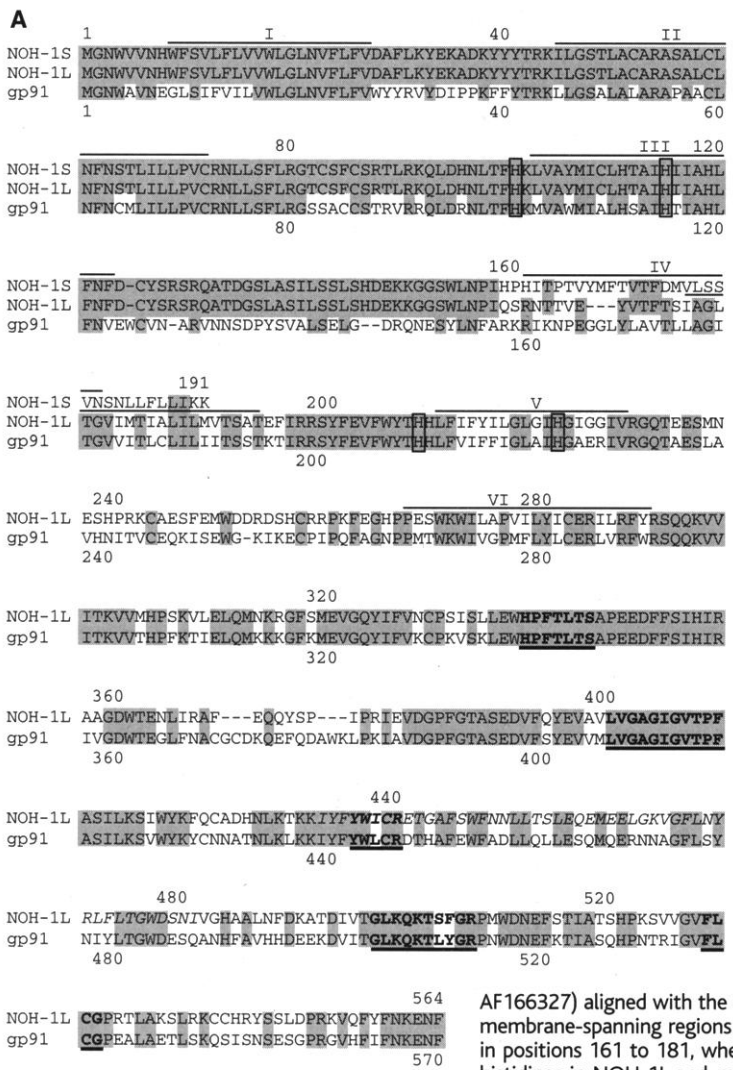

Fig. 3. Structure of *NOH-1* and sequence comparison. (**A**) The deduced amino acid sequence of NOH-1S (GenBank accession number AF166326) and NOH-1L (GenBank accession number AF166327) aligned with the sequence of gp91^{phox}. Shaded boxes indicate identical residues. Presumed membrane-spanning regions are overlined. The fourth transmembrane region of NOH-1S is predicted in positions 161 to 181, whereas it is predicted in positions 173 to 193 for NOH-1L. The four boxed histidines in NOH-1L and gp91^{phox} are the conserved heme-spanning residues of heme cytochromes (*31*). The underlined sequences show the FAD-binding region (residues 338 to 344 of gp91^{phox}) and the NADP pyrophosphate, NADP ribose, and NADP 2′-phosphate-binding regions and the nicotinamide C-4 atom approaching site (*32*) (residues 406 to 416, 442 to 446, 504 to 513, and 535 to 538 of gp91^{phox}). The amino acids absent in NOH-1Lv (GenBank accession number AF166328) are in italics (residues 433 to 481). The NOH-1S EST clone (GenBank accession number AI821410) contained the complete coding sequence shown here. (**B**) Model of the transmembrane topology and of putative functional domains of NOH-1S and NOH-1L. The transmembrane helices, NH_2- and COOH-termini, conserved histidines, and FAD and NADPH binding sites are indicated.

myotubes (*22*). The amino acid sequences of the three *NOH-1* products, NOH-1S (short), NOH-1L [long (*23*)], and NOH-1Lv (long variant, corresponding to the 1.6-kb PCR product), are shown in Fig. 3A (*24*). With the use of a ribonuclease (RNase) protection assay (*25*), NOH-1L was detected in colon, uterus, prostate, and CaCo-2 cells, whereas NOH-1S was detected only in colon and CaCo-2 cells (Fig. 2, A and B). The positive NOH-1S PCR results were confirmed by nested PCR and by sequencing (*22*), which suggested that NOH-1S was indeed present in HL-60 cells and leukocytes but in amounts below the detection threshold of the RNase protection assay.

On the basis of the sequence information, we identified the exons of *NOH-1* gene that generate NOH-1S and NOH-1L (Fig. 1). Exons 1 to 5 code for the common NH_2-terminal 158 amino acids of NOH-1L and NOH-1S. Exons 6 to 13 code for the COOH-terminal 406 amino acids of NOH-1L, with exon 11 missing in NOH-1Lv. Finally, exon 14 codes for the COOH-terminus of NOH-1S. Note that the splice donor site for the generation of NOH-1S is not located at the end of exon 5, but within the exon. The gp91^{phox} gene *CYBB* localizes to the short arm of the X chromosome (Xp21). The size of the corresponding exons is conserved between *NOH-1* and *CYBB*, with the exception of exon 14, for which no corresponding sequence in *CYBB* is known. However, the lengths of the introns are markedly different. Thus, the presence of the two homologous genes is most likely due to a relatively ancient gene duplication.

Hydropathy plots showed a similar profile for NOH-1L and gp91^{phox} (*22*). Predicted transmembrane topology models of NOH-1L and NOH-1S are shown in Fig. 3B. NOH-1L appears similar to gp91^{phox}, with a short cytosolic NH_2-terminus, six transmembrane domains, and a long cytosolic COOH-terminus. NOH-1S shares the cytosolic NH_2-terminus and the first three transmembrane domains with NOH-1L, but terminates with a distinct fourth transmembrane domain followed by a short, intracellular COOH-terminus. NOH-1L contains a heme-spanning histidine motif as well as flavin adenine dinucleotide (FAD) and NADPH binding regions, consistent with its oxidoreductase function (*23*). In contrast, NOH-1S only retains the histidine-rich transmembrane motif postulated to generate voltage-dependent H^+ currents (Fig. 3B).

To investigate whether NOH-1S functions as an H^+ channel, we stably expressed the protein in HEK-293 cells and chose experimental conditions to isolate H^+ currents (*4, 5, 26*). In the absence of a cell line completely devoid of H^+ currents, HEK-293 cells provided a good expression system, as they had only very small H^+ currents (Fig. 4, B and D) and did not express the *NOH-1* isoforms (Fig. 2A). Cells were acidified through the patch pipette to maximize H^+ currents, and depolarizing voltage pulses were applied. No currents above background levels were observed in HEK-293 cells stably transfected with the empty vector (mock-transfectants) or with an unrelated channel protein, hTRP4 (Fig. 4). In contrast, voltage-dependent outward currents were observed in two independent NOH-1S–expressing clones. The currents activated slowly upon depolarization,

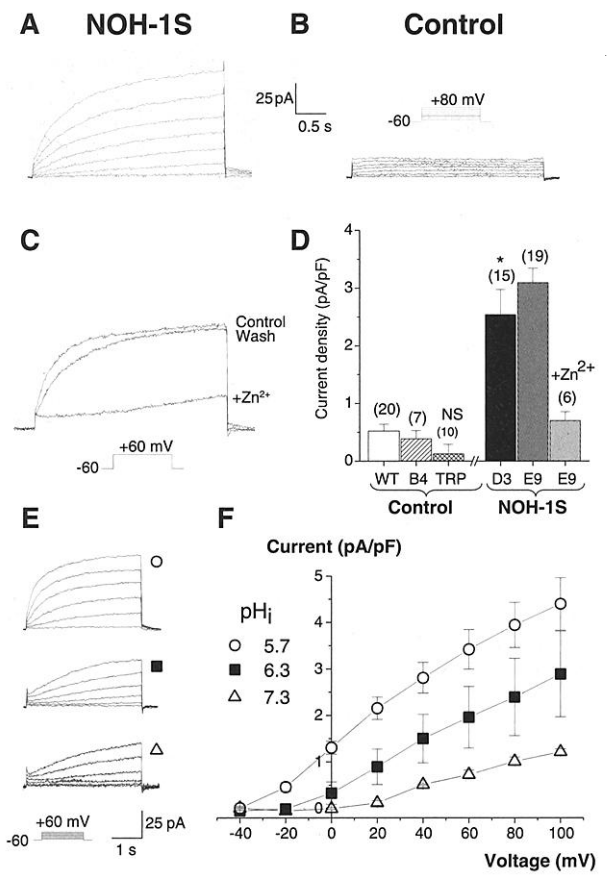

Fig. 4. Cells expressing NOH-1S have voltage-activated, pH-dependent, Zn^{2+}-sensitive currents. (**A** and **B**) Currents in NOH-1S–expressing cells and in mock-transfected cells, elicited by 3-s depolarizing voltage steps ranging from −40 to +80 mV (inset); pH_i 5.7, pH_o 7.5. (**C**) The currents in NOH-1S–expressing cells were reversibly inhibited by 100 μM Zn^{2+}. (**D**) Current densities in wild-type cells (WT) and clones transfected with the empty vector (B4), a calcium channel (hTRP4), or NOH-1S (D3, E9). Zn^{2+} (100 μM) reduced the currents to background levels in NOH-1S–expressing cells. Data are means ± SE of leak-subtracted currents measured at +60 mV, pH_i/pH_o 5.7/7.5 (NS: not significant versus WT; $*P < 0.00004$ versus WT, unpaired t test). (**E**) Families of currents recorded at the indicated pipette pH values in NOH-1S–expressing cells (pH_o 7.5). (**F**) Current-voltage relation of the *NOH-1*–dependent currents recorded at the indicated pipette pH values (means ± SE from 5 to 19 individual cells).

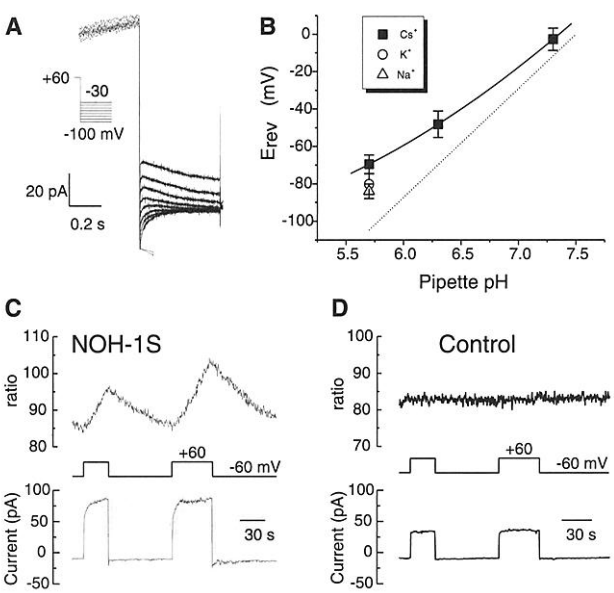

Fig. 5. The NOH-1S currents are H^+ selective and alter cellular pH. (**A**) The reversal potentials of tail currents were measured upon depolarization to various test potentials after a 2-s depolarization to +60 mV (pH_i 5.7, pH_o 7.5). (**B**) Reversal potentials measured in solutions containing Cs^+, Na^+, or K^+, plotted against pipette pH; pH_o 7.5. Values are means ± SE of 3 to 12 experiments. The dotted line shows the H^+ equilibrium potential. (**C** and **D**) Combined recordings of whole-cell currents and of cytosolic pH, measured with carboxy–SNARF-1 in NOH-1S and mock-transfected HEK-293 cells. Long-lasting depolarizing steps to +60 mV were applied (middle), and the currents (bottom) and cytosolic pH changes (top) were measured concomitantly (pH_i 6.5, pH_o 7.5). Cytosolic pH changes were measured with carboxy-SNARF-1 as described (*4*). HEK-293 cells were incubated with 5 μM carboxy–SNARF-1 acetoxymethyl ester for 20 min at room temperature just before recordings in the whole-cell patch-clamp configuration. To compensate for the diffusion of the dye into the patch pipette, we included 100 μM carboxy–SNARF-1 (free acid) in the pipette solution. Data are expressed as the ratio of carboxy-SNARF-1 emission at 640 nm to emission at 580 nm.

and several seconds were required to elicit maximal amplitude, as expected for voltage-dependent H^+ currents of epithelial cells and phagocytes (*27*). The NOH-1S currents were reversibly blocked by Zn^{2+} (100 μM), a known H^+ channel inhibitor (*5*) (Fig. 4C). The experiments are summarized in Fig. 4D. Nontransfected, mock- and hTRP4-transfected cells had only minor currents, whereas cells stably transfected with NOH-1S had large currents that were blocked by Zn^{2+}.

Low intracellular pH generally activates H^+ channels and shifts their threshold of voltage activation toward more negative values. We therefore performed experiments using pipette solutions of differing pH. The amplitudes of the currents were larger and the thresholds of voltage activation were lower as the cytosol was more acidified (Fig. 4, E and F).

The NOH-1S currents share several characteristics of previously described H^+ currents: activation by depolarization and cytosolic acidification, slow kinetics of activation, and reversible block by Zn^{2+}. To directly demonstrate that the observed currents were carried by H^+ ions, we investigated the selectivity of the conductance by tail current analysis. The reversal potential of the current, E_{rev}, depended on the pH gradient and, within the physiological pH range, changed by 46 mV per pH unit (Fig. 5, A and B). At very low pipette pH, E_{rev} deviated from the proton equilibrium potential (E_H) but was not affected by substitution of K^+ or Na^+ in the extracellular solution (Fig. 5B). The 35-mV deviation of E_{rev} from E_H at pH_i 5.7 most likely reflects an imperfect submembranous pH clamp in the presence of large outward currents. However, even assuming that the deviation was due to permeation of other ions, the relative H^+ permeability is still very large [$p_H/p_{Cs} > 10^6$ (*28*)] given the low concentration of H^+ ions. This degree of selectivity is three orders of magnitude higher than Ca^{2+} channels [$p_{Ca}/p_{Cs} = 1:4200$ (*29*)] and in the same range as native H^+ channels (*27*).

Finally, we investigated whether the NOH-1S–associated H^+ channel participates in cytosolic pH homeostasis by measuring intracellular pH during activation of the currents. Cells were patch-clamped in the whole-cell configuration, and cytosolic pH changes were measured with the fluorescent pH indicator carboxy–SNARF-1. As shown in Fig. 5, C and D, the activation of voltage-dependent H^+ currents by long-lasting depolarization from −60 mV to +60 mV led to an increase of cytosolic pH in NOH-1S–expressing cells. In contrast, no pH changes and no H^+ currents above background levels were detected in mock-transfectants. Thus, NOH-1S is able to participate in the regulation of cellular pH and can extrude H^+ ions under intracellular acidic stress.

NOH-1S–expressing HEK-293 cells display electrophysiological properties similar to previously described voltage-gated H^+ channels. On the basis of current kinetics, DeCoursey has suggested the presence of at least four different types of H^+ channels (*27*); the relatively slow time constant of NOH-1S current activation resembles the epithelial type and the phagocyte type. At this point we cannot exclude the possibility that NOH-1S is an H^+ channel regulator, rather than the channel itself. However, H^+ conduction appears to be a general property of several proteins containing an intramembranous histidine motif, as demonstrated by (i) pH measurements in cells expressing full-length or truncated $gp91^{phox}$ (*14–16*), (ii) studies with the mutated Shaker voltage sensor (*9*), and (iii) studies demonstrating H^+ currents in cells expressing NOH-1L and $gp91^{phox}$ (*22*). The fact that NOH-1S does not contain an electron transport chain suggests that H^+ conductance is its main physiological function, whereas flavocytochromes such as NOH-1L or $gp91^{phox}$ might conduct H^+ ions as part of their electron transport mechanism.

Given its limited tissue expression, it is clear that NOH-1S should only be considered as a prototype H^+ channel. We recently identified two additional $gp91^{phox}$ homologs [NOH-2 and NOH-3 (*22*)] that have a high degree of conservation within the histidine-rich third transmembrane domain. Thus, new candidate H^+ channel proteins are already emerging and should provide new insights into H^+ channel heterogeneity.

Note added in proof: A recent publication demonstrates H^+ currents in cells transfected with $gp91^{phox}$ (*33*).

References and Notes

1. We use the consensus terminology "channel" because voltage-dependent H^+ currents mimic several electrophysiological properties of ion channels. However, as previously recognized (*5*), the mechanism of permeation might not necessarily involve a water-filled pore.
2. R. C. Thomas and R. W. Meech, *Nature* **299**, 826 (1982).
3. T. E. DeCoursey, *Biophys. J.* **60**, 1243 (1991).
4. N. Demaurex *et al.*, *J. Physiol. (London)* **466**, 329 (1993).
5. T. E. DeCoursey and V. V. Cherny, *J. Membr. Biol.* **141**, 203 (1994).
6. M. Kuno, J. Kawawaki, F. Nakamura, *J. Gen. Physiol.* **109**, 731 (1997).
7. L. Bernheim *et al.*, *J. Physiol. (London)* **470**, 313 (1993).
8. T. E. DeCoursey and V. V. Cherny, *Biophys. J.* **65**, 1590 (1993).
9. D. M. Starace, E. Stefani, F. Bezanilla, *Neuron* **19**, 1319 (1997).
10. Single-letter abbreviations for amino acid residues are as follows: A, Ala; C, Cys; D, Asp; E, Glu; F, Phe; G, Gly; H, His; I, Ile; K, Lys; L, Leu; M, Met; N, Asn; P, Pro; Q, Gln; R, Arg; S, Ser; T, Thr; V, Val; W, Trp; and Y, Tyr.
11. S. J. Chanock, J. el Benna, R. M. Smith, B. M. Babior, *J. Biol. Chem.* **269**, 24519 (1994).
12. A. W. Segal and K. P. Shatwell, *Ann. N.Y. Acad. Sci.* **832**, 215 (1997).
13. L. M. Henderson, J. B. Chappell, O. T. Jones, *Biochem. J.* **246**, 325 (1987).
14. A. Nanda and S. Grinstein, *Proc. Natl. Acad. Sci. U.S.A.* **88**, 10816 (1991).
15. A. Kapus, K. Szaszi, E. Ligeti, *Biochem. J.* **281**, 697 (1992).
16. L. M. Henderson, G. Banting, J. B. Chappell, *J. Biol. Chem.* **270**, 5909 (1995).
17. L. M. Henderson, *J. Biol. Chem.* **273**, 33216 (1998).
18. A. Nanda, R. Romanek, J. T. Curnutte, S. Grinstein, *J. Biol. Chem.* **269**, 27280 (1994).
19. B. Bánfi *et al.*, *J. Exp. Med.* **190**, 183 (1999).
20. The computation was performed at the ISREC (Lausanne, Switzerland) using the BLAST network service. Applying $gp91^{phox}$ protein fragments (**H**KMVAWMI-AL**H**SAI**H**TIA**H** and HPFTLTSAPEEDFFSIHIRI) (*10*) as queries, we found three human EST clones (AA493362, AI821410 isolated from 12 pooled bulk colon tumors, and AA305700 isolated from CaCo-2 cells). The EST sequences were used as queries for search in the nonredundant DNA database, which yielded the *NOH-1* gene (GenBank accession number Z83819), previously sequenced by D. Lloyd and reported to code a gene similar to the cytochrome b-245 heavy chain.
21. 5′ primers were chosen from exon 1 for NOH-1L and NOH-1S (5′-GCTCCAAACCACCTCTTGAC-3′ and 5′-GAATCTTCCCTGTTGCCTAGAA-3′, respectively); 3′ primers were chosen from exon 13 for NOH-1L and from exon 14 for NOH-1S (5′-TGCAGATTACCGTC-CTTATTCC-3′ and 5′-CACTGTTGGTGTTATATGGG-GA-3′, respectively). Polyadenylated RNA was purified with the Fast Track kit (Invitrogen) from CaCo-2, dimethyl sulfoxide (DMSO)–differentiated HL-60 cells, human peripheral blood leukocytes, and HEK-293 cells. First-strand cDNA was generated using AMV reverse transcriptase (Invitrogen) with random primers. PCR was performed with the Expand High Fidelity PCR System (Boehringer Mannheim) under standard conditions. The products were resolved on 1% agarose gel using ethidium bromide staining.
22. B. Bánfi, A. Maturana, N. Demaurex, K.-H. Krause, data not shown.
23. A recent study describes the cloning of rat and human NOH-1L [referred to as mox-1; Y. A. Suh *et al.*, *Nature* **401**, 79 (1999)] and demonstrates its function as a superoxide-generating NADPH oxidase.
24. The entire coding regions of NOH-1S and NOH-1L were amplified from CaCo-2 cells as in (*21*), but the primers for NOH-1S were 5′-GAATCTTCCCTGTT-GCCTAGAA-3′ and 5′-GAAGAAAATCCTTTATTTTT-TGATGAGC-3′. The PCR products were subcloned into pGEM-T vector (Promega) then into pcDNA3.1 expression vector (Invitrogen) and used to stably transfect HEK-293 cells by the calcium phosphate coprecipitation method. As control, HEK-293 cells were transfected with empty pcDNA3.1 or with a nonrelated channel protein (hTRP4). Transfected cells were selected with G418. Five NOH-1S–transfected clones were analyzed and had currents of >2 pA/pF at +60 mV (pH_i 5.7, pH_o 7.5), whereas none of the three vector-transfected clones displayed currents above background. Two of the NOH-1S–expressing clones and one of the vector-transfected clones, as well as a clone expressing the unrelated channel protein (hTRP4), were selected for detailed analysis.
25. RNase protection assays were carried out with a probe containing the exon 5–exon 14 splice site of NOH-1S (nucleotides 234 to 588 from the start codon), which encompass nucleotides 234 to 473 of NOH-1L. Thus, the protected mRNA fragments are 355 bases long for NOH-1S but 240 bases long for NOH-1L. The glyceraldehyde phosphate dehydrogenase (GAPDH) probe was 125 nucleotides long and protected 97 nucleotides of the relevant mRNA. The riboprobes were transcribed with T7 polymerase. We incubated 10 μg of total RNA from tissues (Clontech) or 500 ng of mRNA from cell lines prepared with the Fast Track kit (Invitrogen) with antisense probe as described [I. Irminger-Finger, J. V. Soriano, G. Vaudan, R. Montesano, A. P. Sappino, *J. Cell Biol.* **143**, 1329 (1998)].
26. Whole-cell patch-clamp recordings were performed in the voltage clamp mode as described (*4*). Pipette resistance was 4 to 12 megohms, seal resistance 5 to 20 gigohms, and access resistance 8 to 30 megohms. The cell capacitance of the different clones was similar and averaged 15.4 ± 0.6 pF (n = 73). Data were filtered at 1 kHz. The time-independent leak currents were subtracted only to calculate the current density.

The bath solution contained 120 mM CsAsp, 1 mM $MgCl_2$, 50 mM Hepes (pH 7.5), and 0.1% glucose; the pipette solution contained 120 mM CsAsp, 1 mM $MgCl_2$, 50 mM MES (pH 5.7 to 6.3) or Hepes (pH 7.3), and 1 mM Mg–adenosine triphosphate (ATP). For the combined current-pH measurements, the pipette solution contained 140 mM CsAsp, 1 mM $MgCl_2$, 10 mM MES (pH 6.5), 1 mM MgATP, and 100 μM carboxy-SNARF-1.

27. T. E. DeCoursey, *Front. Biosci.* **3**, d477 (1998).
28. At $pH_i = 5.7$ and $pH_o = 7.5$, $[H^+]_i = 2 \times 10^{-6}$ M and $[H^+]_o = 3.2 \times 10^{-8}$ M, whereas $[Cs^+]_o = [Cs^+]_i = 0.12$ M. The relative permeability P_H/P_{Cs}, calculated from the reversal potentials with the Goldman-Hodgkin-Katz equation $E_{rev} = RT/F \ln (P_H[H^+]_o + P_{Cs}[Cs^+]_o)/(P_H[H^+]_i + P_{Cs}[Cs^+]_i)$, is 1.18×10^6.
29. B. Hille, *Ionic Channels of Excitable Membranes* (Sinauer, Sunderland, MA, ed. 2, 1992).
30. D. Roos and A. A. Voetman, *Methods Enzymol.* **132**, 250 (1986).
31. L. Yu, M. T. Quinn, A. R. Cross, M. C. Dinauer, *Proc. Natl. Acad. Sci. U.S.A.* **95**, 7993 (1998).
32. D. Rotrosen, C. L. Yeung, T. L. Leto, H. L. Malech, C. H. Kwong, *Science* **256**, 1459 (1992).
33. L. M. Henderson and R. W. Meech, *J. Gen. Physiol.* **114**, 771 (1999).
34. Supported by the Swiss National Science Foundation (K.-H.K., E.L., B.B.), the Max Cloëtta Foundation (N.D.), and the ProRenovanda Cultura Hungariae Foundation (B.B.). We thank L. Mery, W. Schlegel, I. Irminger-Finger, W. Reith, D. Belin, and M. Strubin for helpful discussions, D. P. Lew for continuous support, C. Castelbou and A. Monod for expert help with the transfection and cell culture, and L. Mery for hTRP4-transfected cells.

6 July 1999; accepted 24 November 1999

Stat3-Mediated Transformation of NIH-3T3 Cells by the Constitutively Active Q205L $G\alpha_o$ Protein

Prahlad T. Ram,[1]* Curt M. Horvath,[2] Ravi Iyengar[1]

Expression of Q205L $G\alpha_o$ ($G\alpha_o$*), an alpha subunit of heterotrimeric guanine nucleotide–binding proteins (G proteins) that lacks guanosine triphosphatase (GTPase) activity in NIH-3T3 cells, results in transformation. Expression of $G\alpha_o$* in NIH-3T3 cells activated signal transducer and activator of transcription 3 (Stat3) but not mitogen-activated protein (MAP) kinases 1 or 2. Coexpression of dominant negative Stat3 inhibited $G\alpha_o$*-induced transformation of NIH-3T3 cells and activation of endogenous Stat3. Furthermore, $G\alpha_o$* expression increased activity of the tyrosine kinase c-Src, and the $G\alpha_o$*-induced activation of Stat3 was blocked by expression of Csk (carboxyl-terminal Src kinase), which inactivates c-Src. The results indicate that Stat3 can function as a downstream effector for $G\alpha_o$* and mediate its biological effects.

Although downstream effectors that mediate the actions of G protein α subunits $G\alpha_s$, $G\alpha_i$, and $G\alpha_q$ have been elucidated, little is known about signaling pathways activated by $G\alpha_o$. Expression of the GTPase-deficient (and thus constitutively active) mutant of $G\alpha_o$ in which Gly^{205} is changed to Leu ($G\alpha_o$*) in NIH-3T3 cells results in transformation (*1*), but the molecular mechanisms underlying this phenomenon are not known. MAP kinases 1 and 2 participate in stimulation of proliferation and transformation of NIH-3T3 cells (*2*). The transcription factor Stat3 is activated and required for transformation of NIH-3T3 cells by the v-Src oncogene (*3*). Hence, the roles of MAP kinases and Stat3 in transformation of NIH-3T3 cells by $G\alpha_o$* were investigated.

The Stat family of proteins is implicated in the functions of a wide range of cells (*4*). When activated, Stat3 becomes phosphorylated, dimerizes, and translocates to the nucleus, where it binds DNA and modulates gene expression. To determine the effects of $G\alpha_o$* on the phosphorylation state of native Stat3, we transiently transfected NIH-3T3 cells with a $G\alpha_o$* expression vector, extracted the proteins, resolved them by SDS–polyacrylamide gel electrophoresis (SDS-PAGE), and blotted them with antibodies specific for Stat3 phosphorylated on Tyr^{705} (*5*). Expression of $G\alpha_o$* led to phosphorylation of Tyr^{705} on endogenous Stat3 proteins in NIH-3T3 cells (Fig. 1A). Expression of $G\alpha_o$* did not lead to phosphorylation of Stat1 (*6*). To further determine if the $G\alpha_o$*-induced phosphorylation of Stat3 reflected an increase in Stat3 transcriptional activity, we did a transcriptional activation assay in cells transfected with a Stat3-responsive luciferase reporter construct (*7*). Expression of $G\alpha_o$* resulted in activation of endogenous Stat3 (Fig. 1B), as evidenced by increased reporter gene expression. To determine that the reporter gene activity was in fact due to Stat3 activation, we coexpressed mutant Stat3 proteins that are not phosphorylated or fail to bind DNA and act in a dominant negative manner (*3*). Activation of Stat3 in cells expressing $G\alpha_o$* was inhibited by the coexpression of dominant negative Stat3 proteins (Fig. 1B). Additionally, expression of wild-type $G\alpha_o$ or G protein β and γ subunits had no effect on Stat3 activity (Fig. 1C). Expression of $G\alpha_{12}$* gave a small but consistent twofold increase in Stat3 activity (Fig. 1C). Activation of Stat3 by $G\alpha_q$* was varied (Fig. 1C), and cell density appears to play a role in this activation; further work is being done. Thus, $G\alpha_o$* appears to activate Stat3 in a specific manner in NIH-3T3 cells.

The role of MAP kinases 1 and 2 in cell proliferation and transformation has been extensively studied, and activation of these enzymes can transform NIH-3T3 cells (*2*). Receptor-mediated activation of $G\alpha_o$ leads to increased activity of MAP kinases 1 and 2 in Chinese hamster ovary cells (*8*). Therefore, we examined the effects of $G\alpha_o$* expression on MAP kinase activity in NIH-3T3 cells (*9*). Expression of $G\alpha_o$* did not activate MAP kinases 1 or 2 in NIH-3T3 cells (Fig. 2), as measured by immunoblot analysis with antibodies that specifically recognize the active forms of MAP kinases 1 and 2, which are phosphorylated on Thr^{202} and Tyr^{204}. Thus, the Stat3 signaling pathway and not the MAP kinase 1 and 2 pathway is activated by $G\alpha_o$* in NIH-3T3 cells.

Expression of $G\alpha_o$* transforms NIH-3T3 cells and leads to colony formation in soft agar (*1*). Expression of dominant negative Stat3 inhibits transformation of NIH-3T3 cells by v-Src but not transformation by H-Ras (*3*). To test the hypothesis that activation of Stat3 is necessary for transformation of NIH-3T3 cells by $G\alpha_o$*, we prepared transfected cells that expressed dominant negative Stat3 and $G\alpha_o$* and assayed colony formation (*10*). Expression of dominant negative Stat3 inhibited $G\alpha_o$* transformation of NIH-3T3 cells (Fig. 3). Thus, activation of Stat3 is necessary for transformation of NIH-3T3 cells by $G\alpha_o$*.

Stat3 is activated in response to cytokines and is tyrosine phosphorylated by Janus kinases (JAK) (*11*). We found that expression of $G\alpha_o$* did not activate JAK2 (*6*). However, Stat3 can also be directly phosphorylated and activated by c-Src or v-Src, which results in the proliferation and transformation of several cell types (*3*, *12*). Therefore, we tested whether $G\alpha_o$* activated endogenous c-Src. $G\alpha_o$* was expressed in NIH-3T3 cells. The cells were lysed, endogenous c-Src was immunoprecipitated, and an in vitro kinase assay was done with the immune complex (*13*). Expression of $G\alpha_o$* increased endogenous c-Src activity in NIH-3T3 cells (Fig. 4A). We

[1]Department of Pharmacology, [2]Immunobiology Center, Mount Sinai School of Medicine, One Gustave L. Levy Place, New York, NY 10029, USA.

*To whom correspondence should be addressed. E-mail: ramp01@doc.mssm.edu